

Spherical neutron star collapse in tensor-scalar theory of gravity

Jérôme Novak

*Département d'Astrophysique Relativiste et de Cosmologie
UPR 176 du C.N.R.S., Observatoire de Paris,
F-92195 Meudon Cedex, France*

(July 18, 1997)

Complete tensor-scalar and hydrodynamic equations are presented and integrated, for a self-gravitating perfect fluid, in order to follow the gravitational collapse (including full hydrodynamics) of a neutron star and to study the resulting scalar gravitational wave. During the collapse, only a part of the scalar energy is radiated away as monopolar wave. This wave could be detected by a laser interferometric gravitational wave observatory (such as VIRGO or LIGO), thus constraining the parameters of the theory. The dependence of the wave amplitude and the radiated energy on those parameters is studied and it is shown that there exists some critical value of the parameter of the coupling function between the tensor and the scalar fields, above which these quantities dramatically increase.

PACS number(s): 04.30.Db, 04.50.+h, 04.25.Dm, 02.70.Hm

I. INTRODUCTION

In order to test general relativity, one has to compare it to other, alternative theories of gravitation. *Tensor-scalar* theories, in which gravity is described by a spin-2 field combined with one or several spin-0 fields, are not only alternative theories, but “generalize general relativity” (see [1]); meaning that general relativity is obtained by setting all scalar fields to zero. Several such theories have been developed, from Fierz [2], Jordan [3], Brans and Dicke [4] to Bergman [5], Nordtvedt [6], Wagoner [7] and, more recently, Damour and Esposito-Farèse [1]. In all these theories, the spin-0 and spin-2 fields (φ and $g_{\mu\nu}$) are coupled to matter via an effective metric tensor $\tilde{g}_{\mu\nu} = a^2(\varphi)g_{\mu\nu}$. The Jordan-Fierz-Brans-Dicke theory has only one free parameter ω , whereas for Bergman, Nordtvedt and Wagoner the parameter is a function $\omega(\varphi)$. Damour and Esposito-Farèse considered an arbitrary number of scalar fields, coupled one to the other. All these theories are motivated by, mainly, two theoretical reasons:

1. they represent the low-energy limit of superstring theories ([8] and [9])
2. they give rise to new “extended” inflationary models [10]

Since in Brans-Dicke theory $\log(a(\varphi))$ is a linear function of φ , solar system experiments (weak field) are sufficient to constrain the theory, even in strong fields. Nevertheless, a more general theory, in which $\log(a(\varphi))$ is a parabolic function (depending on two parameters), shows non-perturbative effects in strong field [11], described as “spontaneous scalarization” in [12]. Thus, when describing neutron stars, general relativity and tensor-scalar theory can give significant differences for their masses, radii and gravitational field, whereas the difference can still be negligible in our solar system data. As a consequence, weak-field experiments *cannot* give much information on strong-field regime, and one needs to test this strong-field regime by other means:

- by looking for the orbital decay of binary-pulsar systems. This has been done by Damour and Esposito-Farèse ([1] and [12]), who constrained the parameter space of the coupling function,
- by looking for monopolar gravitational radiation from collapsing compact sources which could be detected by the laser interferometric gravitational wave observatories (such as VIRGO [13] and LIGO [14]).

This latter method requires that the signal be known and that the observed (or unobserved) amplitude can be related to the coupling function parameters. Such kind of computations have already been performed by various groups, but they all considered only an Oppenheimer-Snyder collapse (i.e. “dust” matter, with no pressure), either in Brans-Dicke theory ([15] and [16]) or doing some Taylor expansion of the coupling function [17]. The aim of this paper is to give the results of computations of a spherically symmetric collapse, of a neutron star into a black hole, with one scalar field and an arbitrary coupling function. All the hydrodynamics and field equations are treated with no approximation in order to get the monopolar gravitational wave form and amplitude.

The paper is organized as follow. Section II describes the evolution equations for the star, section III A gives the initial-value models which are evolved by the code described in section III. The results are presented in section IV,

first describing the collapse (IV A), then analyzing the monopolar signal (IV B) and studying the dependence on theory parameters (IV C). Finally, section V gives some concluding remarks.

II. FIELD AND HYDRODYNAMIC EQUATIONS

A. General equations

As it has been stated before, the most general theory containing a spin-2 field and one (massless) spin-0 field contains one arbitrary coupling function $a(\varphi)$. The action is given by

$$S = (16\pi G_*)^{-1} \int d^4x \sqrt{-g_*} (R_* - 2g_*^{\mu\nu} \partial_\mu \varphi \partial_\nu \varphi) + S_m[\Psi_m, a^2(\varphi) g_{\mu\nu}^*] \quad (2.1)$$

where all quantities with a star are related to the “Einstein metric” $g_{\mu\nu}^*$: G_* is the bare gravitational coupling constant, $R_* = g_*^{\mu\nu} R_{\mu\nu}^*$ the curvature scalar for this metric and $g_* = \det(g_{\mu\nu}^*)$. The term S_m denotes the action of the matter, represented by the fields Ψ_m , which is coupled to the “Jordan-Fierz” metric $\tilde{g}_{\mu\nu} = a^2(\varphi) g_{\mu\nu}^*$; all quantities with a tilde are related to this metric. That means that all non-gravitational experiments measure this metric, although the field equations of the theory are better formulated in the Einstein metric. The indices of Einstein frame quantities are moved through Einstein metric, whereas those of Jordan-Fierz quantities are moved through Jordan-Fierz one. By varying S , one obtains

$$R_{\mu\nu}^* - \frac{1}{2} g_{\mu\nu}^* R^* = 2\partial_\mu \varphi \partial_\nu \varphi - g_{\mu\nu}^* g_*^{\rho\sigma} \partial_\rho \varphi \partial_\sigma \varphi + \frac{8\pi G_*}{c^4} T_{\mu\nu}^* \quad (2.2)$$

$$\square_{g_*} \varphi = -4\pi G_* \alpha(\varphi) T_* \quad (2.3)$$

where

$$T_*^{\mu\nu} = \frac{2}{\sqrt{-g_*}} \frac{\delta S_m}{\delta g_{\mu\nu}^*} \quad (2.4)$$

$$\alpha(\varphi) = \frac{\partial \ln a(\varphi)}{\partial \varphi} \quad (2.5)$$

and $\square_{g_*} = g_*^{\mu\nu} \nabla_\mu^* \nabla_\nu^*$ is the Laplace-Beltrami operator of $g_{\mu\nu}^*$, ∇_μ^* denoting the Levi-Civita connection of $g_{\mu\nu}^*$. One can see that $\alpha(\varphi)$ is the basic, field-dependent coupling function between matter and scalar field. General relativity is obtained for $\alpha(\varphi) \rightarrow 0$.

The physical stress-energy tensor $\tilde{T}^{\mu\nu} = 2(-\tilde{g})^{-1/2} \delta S_m / \delta \tilde{g}_{\mu\nu}$ is related to the Einstein-frame one by

$$T_{*\nu}^\mu = a^4(\varphi) \tilde{T}_\nu^\mu \quad (2.6)$$

The equations of motion are given by the stress-energy balance equation, written in the Jordan-Fierz frame

$$\tilde{\nabla}_\nu \tilde{T}_\mu^\nu = 0 \quad (2.7)$$

$$\text{and in the Einstein frame } \nabla_\nu^* T_*^{\mu\nu} = \alpha(\varphi) T_*^\mu \nabla_\mu^* \varphi \quad (2.8)$$

Finally, let us call φ_0 the cosmological value of the scalar field, which enters the theory as the boundary condition on the scalar field at spatial infinity.

B. Coordinates and variables

The present calculations have essentially been done by generalizing a previous work by Gourgoulhon [18] to tensor-scalar theory. Therefore, a very brief presentation of coordinate and variable choice will be given here. The Einstein-scalar equations have been decomposed in the 3+1 formalism [19] onto a family of spacelike hypersurfaces Σ_t labeled by the real index t called the *coordinate time*. The *polar time slicing* has been chosen in order to have good singularity avoidance (see e.g. [20] for discussion). On each hypersurface Σ_t the *radial gauge* has been chosen with spherical-like coordinates (r, θ, ϕ) , since the considered problem is spherically symmetric. All these assumptions (spherical symmetry,

radial gauge and polar slicing) imply that the metric $g_{\mu\nu}^* = a^{-2}(\varphi)\tilde{g}_{\mu\nu}$ (which verifies Einstein-like equations (2.2), with an extra-term) takes the diagonal form:

$$ds^2 = -N^2(r, t)dt^2 + A^2(r, t)dr^2 + r^2(d\theta^2 + \sin^2\theta d\phi^2) \quad (2.9)$$

where $N(r, t)$ is called the *lapse function*. The metric $g_{\mu\nu}^*$ will often be described by the three functions $\nu(r, t)$, $m(r, t)$ and $\beta(r, t)$ defined by

$$N(r, t) = \exp(\nu(r, t)) \quad (2.10)$$

$$A(r, t) = \left(1 - \frac{2m(r, t)}{r}\right)^{-1/2} \quad (2.11)$$

$$\text{and } \beta(r, t) = \ln\left(\frac{N}{A}\right) \quad (2.12)$$

All coordinates are expressed in the Einstein-frame, and stars are omitted. However, “physical” quantities will often be written in the Fierz metric and noted with a tilde.

In this work, neutron stars were modeled as self-gravitating perfect fluids. They can be considered to be made of degenerate matter at equilibrium, the equation of state not depending on temperature (cold matter). This does not hold soon after their formation. The stress-energy tensor writes

$$\tilde{T}_{\mu\nu} = (\tilde{e} + \tilde{p})\tilde{u}_\mu\tilde{u}_\nu + \tilde{p}\tilde{g}_{\mu\nu} \quad (2.13)$$

where \tilde{u}_μ is the 4-velocity of the fluid, \tilde{e} is the total energy density (including rest mass) in the fluid frame and \tilde{p} is the pressure. The relation to its Einstein-frame counterpart is $T_\nu^\mu = a^4(\varphi)\tilde{T}_\nu^\mu$. The description of the fluid is completed by an equation of state

$$\tilde{e} = \tilde{e}(\tilde{n}_B) \quad (2.14)$$

with \tilde{n}_B being the baryonic density in the fluid frame. One then deduces the pressure as a function of \tilde{n}_B . Let $\Gamma = \tilde{N}\tilde{u}^0$ be the Lorentz factor connecting the fluid frame and Σ_t hypersurface frame, calling

$$\tilde{E} = -\tilde{T}_0^0 \text{ one gets } \tilde{E} = \Gamma^2(\tilde{e} + \tilde{p}) - \tilde{p} \quad (2.15)$$

The fluid baryonic number is represented by the *coordinate baryonic density*

$$\tilde{D} = \frac{\text{number of baryons in } \delta V}{\delta V} = A\Gamma\tilde{n}_B \quad (2.16)$$

where $\delta V = r^2 \sin\theta dr d\theta d\phi$ is the element of the coordinate 3-volume on a given Σ_t , defined as the set of points whose coordinates are between r and $r + dr$, θ and $\theta + d\theta$, ϕ and $\phi + d\phi$. The fluid motion is described by the following variables

$$V = \frac{dr}{dt} = \frac{u^r}{u^0} \text{ (coordinate velocity)} \quad (2.17)$$

$$U = \frac{\text{proper distance travelled on } \Sigma_t}{\text{elapsed proper time on } \Sigma_t} = \frac{A}{N}V \quad (2.18)$$

one then has $\Gamma = (1 - U^2)^{-1/2}$ and deduces the components of $\tilde{T}_{\mu\nu}$ given by (2.13). The fluid *log-enthalpy* is also introduced, defined as:

$$H = \ln\left(\frac{\tilde{e} + \tilde{p}}{\tilde{n}_B m_B c^2}\right) \quad (2.19)$$

and, finally, three “scalar-field” variables:

$$\eta = \frac{1}{A} \frac{\partial \varphi}{\partial r} \quad (2.20)$$

$$\psi = \frac{1}{N} \frac{\partial \varphi}{\partial t} \quad (2.21)$$

$$\Xi = \eta^2 + \psi^2 \quad (2.22)$$

C. Tensor-scalar field equations

Spherical symmetry helps to obtain gravitational field equations; we followed the procedure described by Gourgoulhon [18], projecting eqs. (2.2–2.3) on the 3-surfaces Σ_t and along their normal. Hereafter, we use the following notation:

$$q_\pi = \frac{8\pi G_*}{c^4}$$

The tensor Einstein-like equations (2.2) turn then into:

– one *Hamiltonian constraint equation*

$$\frac{\partial m}{\partial r} = r^2 \frac{c^2}{2G_*} \left(\Xi + q_\pi a^4(\varphi) \tilde{E} \right) \quad (2.23)$$

– three *momentum constraint equations* which reduce to only one non-vanishing

$$\frac{\partial m}{\partial t} = r^2 \frac{c^2}{2G_*} \left[2 \frac{N}{A} \psi \eta - q_\pi a^4(\varphi) (\tilde{E} + \tilde{p}) \tilde{V} \right] \quad (2.24)$$

– six *Einstein dynamical equations* which here reduce to two non-vanishing; one is degenerate, only giving a condition on the lapse function

$$\frac{\partial \nu}{\partial r} = \frac{q_\pi A^2}{2} \left[\frac{mc^2}{4\pi r^2} + r(\tilde{p} + \tilde{U}^2(\tilde{E} + \tilde{p})) + r\Xi \right] \quad (2.25)$$

The other one will not be used in this work.

Writing the scalar-field wave equation (2.3) with our variables gives

$$\frac{\partial^2 \varphi}{\partial t^2} = e^{2\beta} \left(\Delta \varphi + \frac{\partial \beta}{\partial r} \frac{\partial \varphi}{\partial r} \right) + \frac{\partial \beta}{\partial t} \frac{\partial \varphi}{\partial t} - q_\pi \frac{\alpha(\varphi) a^4(\varphi) N^2}{2} (\tilde{E} - 3\tilde{p} - (\tilde{E} + \tilde{p})U^2) \quad (2.26)$$

One more equation concerning the scalar field will be used; although it is redundant with (2.23)–(2.26), from which it is deduced, it will be useful for numerical integration:

$$\frac{1}{2} \frac{\partial \Xi}{\partial t} = \left\{ \frac{N}{A} \left[\psi \Delta \varphi + \eta \frac{\partial \psi}{\partial r} \right] + \frac{2N}{A} \psi \eta \frac{\partial \nu}{\partial r} - \Xi \frac{G_* A^2}{rc^2} \frac{\partial m}{\partial t} \right\} + \psi q_\pi \alpha(\varphi) a^4(\varphi) N (\tilde{E} - 3\tilde{p} - (\tilde{E} + \tilde{p})U^2) \quad (2.27)$$

D. Matter evolution equations

In order to get the evolution of the variables \tilde{E} and U , let us consider the momentum-energy conservation equation (2.8), we get

$$\frac{\partial \tilde{E}}{\partial t} + \frac{1}{r^2} \frac{\partial}{\partial r} (r^2 (\tilde{E} + \tilde{p}) V) = -(\tilde{E} + \tilde{p}) \left\{ \alpha(\varphi) N [(3 + U^2)\psi + 4U\eta] + rAN [(1 + U^2)\psi\eta + U\Xi] \right\} \quad (2.28)$$

$$\frac{\partial U}{\partial t} + V \frac{\partial U}{\partial r} = -\frac{1}{\tilde{E} + \tilde{p}} \left(U \frac{\partial \tilde{p}}{\partial t} + \frac{N}{A} \frac{\partial \tilde{p}}{\partial r} \right) - \frac{AN}{\Gamma} \left[\frac{G_* m}{r^2 c^2} + q_\pi a^4(\varphi) \frac{r\tilde{p}}{2} + \frac{\alpha(\varphi)}{A} (\eta + U\psi) + rU\eta\psi + \frac{r}{2}\Xi \right] \quad (2.29)$$

Equation (2.28) expresses the total energy conservation (matter plus gravitational and scalar energy), eq. (2.29) being the tensor-scalar analogous of the Euler equation. One notes, in the latter, the $\frac{1}{\tilde{E} + \tilde{p}} \left(U \frac{\partial \tilde{p}}{\partial t} + \frac{N}{A} \frac{\partial \tilde{p}}{\partial r} \right)$ term which may cause some trouble when numerically calculating it, since it is the quotient of two quantities vanishing at the surface of the star. Thus, if one uses the log-enthalpy (2.19), this term may be replaced by $\frac{1}{\Gamma^2} \left(U \frac{\partial H}{\partial t} + \frac{N}{A} \frac{\partial H}{\partial r} \right)$, which is well defined near the surface.

Expressing the baryonic number conservation

$$\tilde{\nabla}_\mu \tilde{n}_B \tilde{u}^\mu = 0 \quad (2.30)$$

one obtains

$$\frac{\partial \tilde{D}}{\partial t} + a(\varphi) \frac{1}{r^2} \frac{\partial}{\partial r} (r^2 \tilde{D} V) + \alpha(\varphi) \tilde{D} N (3\psi + 4U\eta) = 0 \quad (2.31)$$

Because log-enthalpy is used in order to avoid numerical singularities at the surface, there has to be an evolution equation of that quantity. Since $H = H(\tilde{n}_B)$, and $\tilde{n}_B = \frac{\tilde{D}}{A\Gamma}$, one may write

$$\begin{aligned} \frac{\partial H}{\partial t} + V \frac{\partial H}{\partial r} &= \frac{\partial H}{\partial \tilde{n}_B} \left(\frac{\partial \tilde{n}_B}{\partial t} + V \frac{\partial \tilde{n}_B}{\partial r} \right) \\ &= \frac{\partial H}{\partial \tilde{n}_B} \frac{V}{A\Gamma} (1 - a(\varphi)) \frac{\partial \tilde{D}}{\partial r} - \tilde{n}_B \frac{\partial H}{\partial \tilde{n}_B} \left[\frac{1}{r^2} \frac{\partial}{\partial r} (r^2 V) + \alpha(\varphi) N (3\psi + 4U\eta) \right. \\ &\quad \left. + \frac{1}{A} \left(\frac{\partial A}{\partial t} + V \frac{\partial A}{\partial r} \right) + \Gamma^2 U \left(\frac{\partial U}{\partial t} + V \frac{\partial U}{\partial r} \right) \right] \end{aligned} \quad (2.32)$$

with terms in the right-hand side being replaced using eqs. (2.23), (2.24) and (2.29) by source terms involving \tilde{E}, \tilde{p} and Ξ . The numerical evolution of all these equations (2.23)–(2.32) will be presented in next section.

III. TESTS AND NUMERICAL PROCEDURE

All previous equations have been checked using a Mathematica algebraic code. More precisely, the Schwartz relation for equations (2.23) and (2.24)

$$\frac{\partial^2 m}{\partial r \partial t} - \frac{\partial^2 m}{\partial t \partial r} = 0$$

has been computed and one then gets

$$\frac{\partial \varphi}{\partial t} \times (\square_{g_*} \varphi + q_\pi \alpha(\varphi) T_*) = \frac{\partial \tilde{E}}{\partial t} + \frac{1}{r^2} \frac{\partial}{\partial r} (r^2 (\tilde{E} + \tilde{p}) V) - \left(\text{right-hand side of eq. (2.28)} \right)$$

which is consistent with (2.26) and (2.28). Finally, setting $\varphi = 0$ gives the equations of general relativity as described in [18].

A. Static configurations

Physical scenarios to form a black hole involve either an accreting neutron star or a post-supernova remnant (when a part of the ejected envelop falls back onto the new-born neutron star). In both cases, the mass of the neutron star must reach its maximal value above which the star becomes unstable. It is then interesting to get unstable equilibrium configurations of neutron stars, endowed with a scalar field, close to the maximal mass. They are used as initial configurations for the collapse. Thus, setting all $\partial/\partial t$ terms, V and U to zero in eqs. (2.23)–(2.28), one gets the scalar equivalent of the Tolman-Oppenheimer-Volkoff system. The system obtained is the same as equations (7) in [11], since the same gauge is used. Therefore, the following test was performed: considering the same equation of state (polytrope $\gamma = 2.34$ and $K = 0.0195$, hereafter called EOS1), the same coupling function ($a(\varphi) = \exp(-3\varphi^2)$) and asymptotic scalar field value ($\varphi_0 = 0.0043$), we obtained the same dependence for the effective scalar coupling constant (the ratio between the scalar and the gravitational energies) on the star's baryonic mass (Fig.2 of [11] and Fig. 1 of this work). We also observed an increase of the maximal gravitational mass of neutron stars, when taking into account the scalar field, as it has been showed in Fig. 1 of [11].

Considering a polytropic equation of state

$$\begin{aligned} \tilde{e}(\tilde{n}_B) &= \tilde{n}_B \tilde{m}_B + K \frac{\tilde{n}_0 \tilde{m}_B}{\gamma - 1} \left(\frac{\tilde{n}_B}{\tilde{n}_0} \right)^\gamma \\ \tilde{p} &= K \tilde{n}_0 \tilde{m}_B \left(\frac{\tilde{n}_B}{\tilde{n}_0} \right)^\gamma \end{aligned} \quad (3.1)$$

with $\tilde{m}_B = 1.66 \times 10^{-27} \text{kg}$ and $\tilde{n}_0 = 0.1 \text{fm}^{-3}$, one can integrate the scalar TOV system, starting at the center with a given value for $\tilde{n}_B(r=0)$, up to the surface at which $\tilde{n}_B(r=r_{star})=0$. The total ADM mass of $g_{\mu\nu}^*$, which will be called *gravitational mass* and the total scalar charge ω such that, for $r \rightarrow \infty$, $\varphi(r) = \varphi_0 + G_*\omega/r + O(1/r^2)$, can be determined through eqs.(8) of [11]. These two quantities are then useful to match the obtained interior solution to the exterior one (spherically symmetric solution in vacuum), which is known analytically in an other gauge (described in [21]) and thus one can obtain a static solution everywhere. The results are shown in Fig. 2, with large value of the scalar field, even for a very small asymptotic field φ_0 . These solutions are then used as initial values for the dynamical evolution. They have been computed, with increasing central densities $\tilde{n}_B(r=0)$, in order to get an unstable configuration (for which gravitational mass is a decreasing function of the density). Then, the dynamical code is sensitive enough to trigger the instability only by round-off errors. The hydrostatic equilibrium is obtained, thanks to pseudo-spectral techniques [22], up to very high accuracy (10^{-10} relative error on the hydrostatic equilibrium), which enables the dynamical code to be sensitive to instability (see [18]).

B. Wave equation

The evolution of the scalar field is given by (2.26), which has been numerically treated as a wave equation, with extra source terms

$$\begin{aligned} \frac{\partial^2 \varphi}{\partial t^2} &= \Delta \varphi + \sigma_\varphi \\ \text{with} \\ \sigma_\varphi &= (e^{2\beta} - 1) \Delta \varphi + e^{2\beta} \frac{\partial \beta}{\partial r} \frac{\partial \varphi}{\partial r} + \frac{\partial \beta}{\partial t} \frac{\partial \varphi}{\partial t} + (\text{Matter source terms}) \end{aligned}$$

This equation is then integrated, using a pseudo-spectral technique for spatial operators, on a semi-implicit second-order integration scheme, as described for the 3-D case by Bonazzola and Marck [23]. The boundary condition imposed on the outer edge of the grid (far away from the star) is that of an *outgoing wave*, meaning that the wave can be written as

$$\varphi(t, r) = \varphi_0 + \frac{1}{r} F(t - \frac{r}{c}) \quad (3.2)$$

which is an exact condition for 1-D waves. Differentiating, one gets

$$\left. \frac{1}{c} \frac{\partial \varphi}{\partial t} + \frac{\partial \varphi}{\partial r} + \frac{(\varphi - \varphi_0)}{r} \right|_{\text{outer edge}} = 0 \quad (3.3)$$

Actually, this is not the right boundary condition for our wave equation on curved space-time, however, since the boundary condition is imposed far away from the star (i.e. on a nearly flat space-time), a good approximation is obtained by taking as a boundary condition

$$\left. e^{-\beta} \frac{\partial \varphi}{\partial t} + \frac{\partial \varphi}{\partial r} + \frac{\varphi}{r} \right|_{\text{outer edge}} = 0 \quad (3.4)$$

The numerical code has been checked by taking analytical solutions of simpler wave equations $\partial^2 \varphi / \partial t^2 = H(t, r)^2 \Delta \varphi$, and verifying that the discrepancy between numerical solution and the analytical one goes down as the square of the integration time step (second order scheme). The boundary condition has been checked by looking for the remaining energy of the wave in the grid, after the wave was supposed to be “gone out”. As it will be seen in next section, a numerical grid partly comoving with the fluid will be used. For this purpose, the wave equation have been adapted to such a grid and tested.

C. Dynamical evolution

The integration procedure is quite similar to that of Gourgoulhon in [18]. All matter and field quantities are supposed to be known at some initial instant t_0 , and one wants then to get them at $t_0 + \delta t$. First, one can compute the scalar field variables φ and Ξ at that time thanks to wave equation (2.26) and eq. (2.27). Similarly, one gets the fluid quantities \tilde{E} , U (and thus Γ), H and \tilde{D} , with their evolution equations (2.28), (2.29), (2.32) and (2.31).

Then, one can deduce the metric coefficient $A(r, t_0 + \delta t)$ through eq. (2.23) and (2.11) and determine the fluid proper baryonic density \tilde{n}_B , by inverting relation (2.16). The equation of state then gives the pressure $\tilde{p}(\tilde{n}_B)$. Here, one has a good test of the accuracy by comparing \tilde{e} given by the equation of state with that deduced from \tilde{E} (evolved). The same is possible for H .

Finally, one uses eq. (2.25) to obtain $\nu(r, t_0 + \delta t)$, which is determined up to an additive constant. Since there is no Birkhoff Theorem in scalar-tensor gravity, this constant cannot be determined by matching the interior solution to the exterior (static) one, used before. Even the exterior space-time is dynamic. Using a large grid (which is going far away from the star) enables to be in weak-field regime at the outer edge of the grid and so, to write with a good approximation

$$\forall t, A(R_{out}, t) \times N(R_{out}, t) = \text{Constant} \quad (3.5)$$

the constant being determined for the static configuration. Observing $A(R_{out})$ during the collapse, one sees that $\Delta A(R_{out}) \leq 10^{-5}$. This is quite lower than the overall committed error, which is deduced from the discrepancy between \tilde{E} (evolved) and \tilde{e} (obtained from the equation of state) and is $\sim 10^{-3}$. Once $N(r, t)$ is obtained, the velocity V is deduced and all quantities are known at the instant $t_0 + \delta t$.

As far as the numerical work is concerned, the code is based on pseudo-spectral methods, the spatial part of the functions being expanded on a set of Chebychev polynomials on a multi-zone grid. Time integration is then performed with a second-order semi-implicit scheme, boundary conditions being imposed on the H, U system

$$\left. \frac{1}{r^2} \frac{\partial}{\partial r} r^2 V \right|_r = R_{star} = 0 \quad (3.6)$$

and on the wave equation (3.4). The grid is partly comoving with the fluid, meaning that in each zone inside the star, both edges are comoving, the grid's velocity at each point being (linearly) interpolated. The edge of the outer zone is at rest ($V_{grid}(r = r_{out}) = 0$), and the grid's velocity between star's surface and this outer edge is interpolated at each point the same way. The equation of state used in this work is always polytropic: either EOS1, or $\gamma = 2$ and $K = 0.001$, called EOS2. For more details on the numerical procedure, see [18], [22], [23] and [24]. Contrary to [18], a multi-zone (multi-grid) expansion is done. Typically, two zones have been used for the star's interior and three for the exterior, with about 65 points in each zone, which is considerably lower than the number of points used in finite difference schemes. A full run took about 20 minutes of CPU time on an Onyx Silicon Graphics workstation, for ~ 20000 time steps.

IV. NUMERICAL RESULTS

An important choice is that of the coupling function $a(\varphi)$. Following [12], we chose a function depending on two parameters, for all our study:

$$a(\varphi) = e^{\alpha_0(\varphi - \varphi_0) + \frac{\beta_0}{2}(\varphi - \varphi_0)^2} \quad (4.1)$$

Figure 9 of [12] gives constraints on the (α_0, β_0) space of parameters, imposed by binary-pulsar measurements. Section IV C investigates this space of parameters for scalar gravitational waves.

A. Description of the collapse

Hereafter, three collapses will be presented, called A, B, C and D. The parameters of the static configurations, which were used as initial conditions for the collapse, are described in table I. Note that collapses A and B use a $\gamma = 2.34$ polytrope, whereas C and D use a $\gamma = 2$ one. First, only the case A will be considered. As far as the hydrodynamic part is concerned, the collapse is very similar to that in general relativity, described in [18]. It can be seen from Fig. 3, that an apparent horizon appears at $r = r_{star}$ ($A(r_{star}) \rightarrow \infty$). On that figure are plotted all quantities from the beginning to the end of the collapse (when $N(r = 0)$ becomes too small). For $r < r_{star}$, one notices that the lapse goes to zero. Since all evolution equations are written $\partial/\partial t = N \times (\text{source term})$ and the coordinate velocity $V = (N/A) U \rightarrow 0$, all hydrodynamic and scalar-field quantities are “frozen” inside the star's surface. Therefore, their evolution can be numerically stopped, when the lapse had become sufficiently small ($N \sim 10^{-5}$), in order to avoid the singularity of $A(r = r_{star})$. However, all field quantities continue to evolve *outside* the star. The results are shown in Fig. 4. The fate of the scalar field is particularly interesting:

- for $r < r_{star}$ the field is “frozen” inside what will become an apparent horizon; a certain amount of scalar energy will be swallowed into the (future) black hole,
- for $r > r_{star}$ the field relaxes toward the asymptotic constant value set by cosmological evolution; the other part of scalar energy of the star is radiated away as scalar gravitational wave.

The results are quite different from those of [16] who find that, in Brans-Dicke theory, all the scalar mass is radiated away. Since our code use polar slicing to have a diagonal metric, it is not able to handle the collapse up to the final stage and this final stage cannot be fully described. Nevertheless, the behavior of all the fields outside the star *seems* to indicate that the final state is a Schwarzschild black hole surrounded by a constant scalar field.

B. Scalar gravitational waves

It has been seen, in the previous section, that the main difference from general relativity is the scalar monopolar radiation, which carries away energy and can interact with a detector. Looking far from the source (at a distance r), one can write the metric (see [1])

$$\tilde{g}_{\mu\nu} = a^2(\varphi_0) \left[\eta_{\mu\nu} + \frac{1}{r} (h_{\mu\nu}^* + 2\alpha_0 F \eta_{\mu\nu}) + O(r^{-2}) \right] \quad (4.2)$$

where $\eta_{\mu\nu}$ is the flat metric, $h_{\mu\nu}^*(t)$ and $F(t)$ are respectively the quadrupolar and monopolar components of the wave. Since this work is done in spherical symmetry, only the monopolar mode shall be considered. The function $F(t)$ is the same as that of eq. (3.2), setting r constant. It is the quantity

$$h(t) = \frac{2}{D} a^2(\varphi_0) \alpha_0 F(t) \quad (4.3)$$

where D is the distance between the source and the detector, which could be detected by interferometric gravitational wave observatories (as VIRGO or LIGO), see [1], [17] or [25]. The radiated energy writes

$$E_{scal} = \frac{c}{G_*} \int_0^{+\infty} \left(\frac{dF}{dt} \right)^2 dt \quad (4.4)$$

and one can notice that this latter does not depend on the parameter α_0 , whereas h is directly proportional to it. Thus, E_{ray} is much more sensitive to β_0 .

The shape of h is immediately obtained from the shape of φ , far from the source (Fig. 4) and is qualitatively similar to those found in [15] and [16]. The Fourier spectrum of the signal is

$$\tilde{h}(f) = \int_0^{t_{max}} h(t) e^{2\pi i f t} dt \quad (4.5)$$

but the quantity which can be compared with the root mean square of the detector noise is $f|\tilde{h}|$, and is plotted in Fig. 5, for the collapse A. The signal (at 1 Mpc) is quite below the sensitivity of the detectors, due to a very small parameter α_0 . Solar-system experiments and binary pulsar constraints tell us $\alpha_0 < \text{few} \times 10^{-2}$ (see [12]). The power spectrum of the signal for the collapse B is shown in Fig. 6, with a larger α_0 . The shape is the same, but the amplitude is considerably higher, therefore, the study of the parameter space (α_0, β_0) can be reduced and one has to pay more attention to β_0 than to α_0 . Finally, similarities between these spectra and those of Shibata et al. give high confidence in both works.

C. Exploration of the parameter space

Up to now, only one equation of state has been used; collapse C has been performed with EOS2 (see sect. III C). Results are shown in Figs. 7 and 8 and are similar to those of EOS1 (collapses A and B), the scalar gravitational wave signal having the same shape. This is better seen on Fig. 9, with the Fourier spectrum being close to that of collapse B. Thus, varying the parameters of the polytropic equation of state is not of much interest. Better would be the use of a realistic equation of state (as in [18]) but, for this work, a polytrope gives already good results.

The parameter β_0 has not yet been changed. From previous works [11] and [12], one can see that it can dramatically change the amount of scalar energy in a star (“spontaneous scalarization”). Many runs have been performed with β_0 varying from 0 to -6. The scalar gravitational wave amplitude and radiated energy have been plotted for each of these runs on Figs. 10 and 11. One notices the sudden increase of both quantities for β_0 lower than some critical value; this is less visible when considering a larger α_0 . For $\alpha_0 = 10^{-5}$ the critical value of $\beta_0 = -5.1$, for $\alpha_0 = 10^{-2}$, it is $\beta_0 = -4.5$. These values are easier to see if normal (linear) graphs are used instead of logarithmic ones.

V. CONCLUSIONS

This work has been done with very few approximations ($A \times N = C^{te}$ at the outer edge of the grid, evolution “frozen” when the lapse becomes too small); all the tensor-scalar equations, including hydrodynamics, are solved with high accuracy by means of spectral methods. The results compare well with those of previous (simplified) similar works. Mainly, one sees that the outgoing monopolar gravitational wave is very dependent on the coupling function, especially the β_0 parameter. This is interesting because the α_0 parameter can be constrained by solar-system experiments, since it represents only a linear deviation from general relativity, whereas β_0 cannot be really probed by that mean. The signal being in the bandwidth and above the sensitivity of the interferometric detectors currently under construction, it represents an interesting way to constrain tensor-scalar theories. A future project of study is the supernova collapse and bounce in this framework since, in that case, one has electromagnetic and neutrino signals which make possible the use of even negative results of detection.

ACKNOWLEDGMENTS

I thank Thibault Damour for suggesting to do this work, and for fruitful discussions. I am very grateful to Ericourgoulhon for help, discussions and careful reading of the manuscript. The numerical calculations have been performed on Silicon Graphics workstations purchased thanks to the support of the SPM department of the CNRS and the Institut National des Sciences de l’Univers.

-
- [1] T. Damour and G. Esposito-Farèse, *Class. Quantum Grav.* **9**, 2093 (1992)
 - [2] M. Fierz, *Helv. Phys. Acta* **29**, 128 (1956)
 - [3] P. Jordan, *Z. Phys.* **157**, 112 (1959)
 - [4] C. Brans and R.H. Dicke, *Phys. rev.* **124**, 925 (1961)
 - [5] P.G. Bergmann, *Int. J. Theor. Phys.* **1**, 25 (1968)
 - [6] K. Nordtvedt, *Astrophys. J.* **161**, 1059 (1970)
 - [7] R.V. Wagoner, *Phys. Rev. D* **1**, 3209 (1970)
 - [8] C.G. Callan, D. Friedman, E.J. Martinec and M.J. Perry, *Nucl. Phys. B* **262**, 593 (1985)
 - [9] T. Damour and A.M. Polyakov, *Nucl. Phys. B* **423**, 532 (1994)
 - [10] P.J. Steinhardt and F.S. Accetta, *Phys. Rev. Lett.* **64**, 2740 (1990)
 - [11] T. Damour and G. Esposito-Farèse, *Phys. Rev. Lett.* **70**, 2220 (1993)
 - [12] T. Damour and G. Esposito-Farèse, *Phys. Rev. D* **54**, 1474 (1996)
 - [13] C. Bradaschia, *et al.*, *Science* **256**, 325 (1992)
 - [14] K.S. Thorne, in *Proceedings of the International Conference on Particle Physics, Astrophysics and Cosmology* (1996), p41
 - [15] M. Shibata, K. Nakao and T. Nakamura, *Phys. Rev. D* **50**, 6058 (1994)
 - [16] M.A. Scheel, S.L. Shapiro and S.A. Teukolsky, *Phys. Rev. D* **51**, 4236 (1995)
 - [17] T. Harada, T. Chiba, K. Nakao and T. Nakamura, *Phys. Rev. D* **55**, 2024 (1997)
 - [18] E.ourgoulhon, *Astron. Astrophys.* **252**, 651 (1991)
 - [19] R. Arnowitt, S. Deser and C.W. Misner, in *Gravitation* Witten L. (ed.) Wiley, New York (1962)
 - [20] T. Piran, in *Rayonnement gravitationnel – Les Houches 1982* N. Deruelle and T. Piran (eds.) North Holland, Amsterdam (1983)
 - [21] R. Coquereaux and G. Esposito-Farèse, *Ann. Inst. H. Poincaré* **52**, 113 (1990)
 - [22] S. Bonazzola and J.A. Marck, *Astron. Astrophys.* **164**, 300 (1986)
 - [23] S. Bonazzola and J.A. Marck, *J. Comp. Phys.* **87**, 201 (1990)

- [24] S. Bonazzola, E. Gourgoulhon and J.A. Marck, in *Relativistic Gravitation and Gravitational Radiation* J. A. Marck and J. P. Lasota (eds.) Cambridge University Press (in press)
- [25] R.V. Wagoner and D. Kalligas, in *Relativistic Gravitation and Gravitational Radiation* J. A. Marck and J. P. Lasota (eds.) Cambridge University Press (in press)

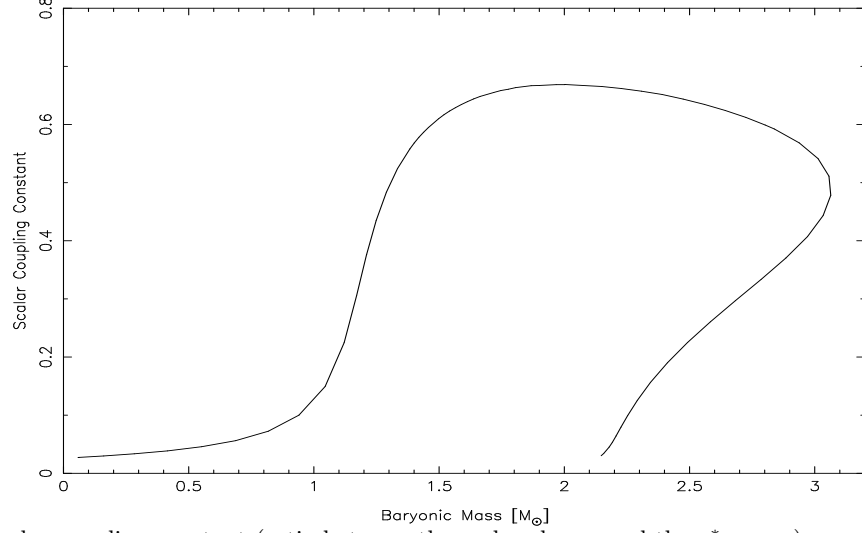


FIG. 1. Effective scalar coupling constant (ratio between the scalar charge and the $g_{\mu\nu}^*$ mass) versus the baryonic mass for EOS1 neutron stars, with a coupling function $a(\varphi) = \exp(-3\varphi^2)$

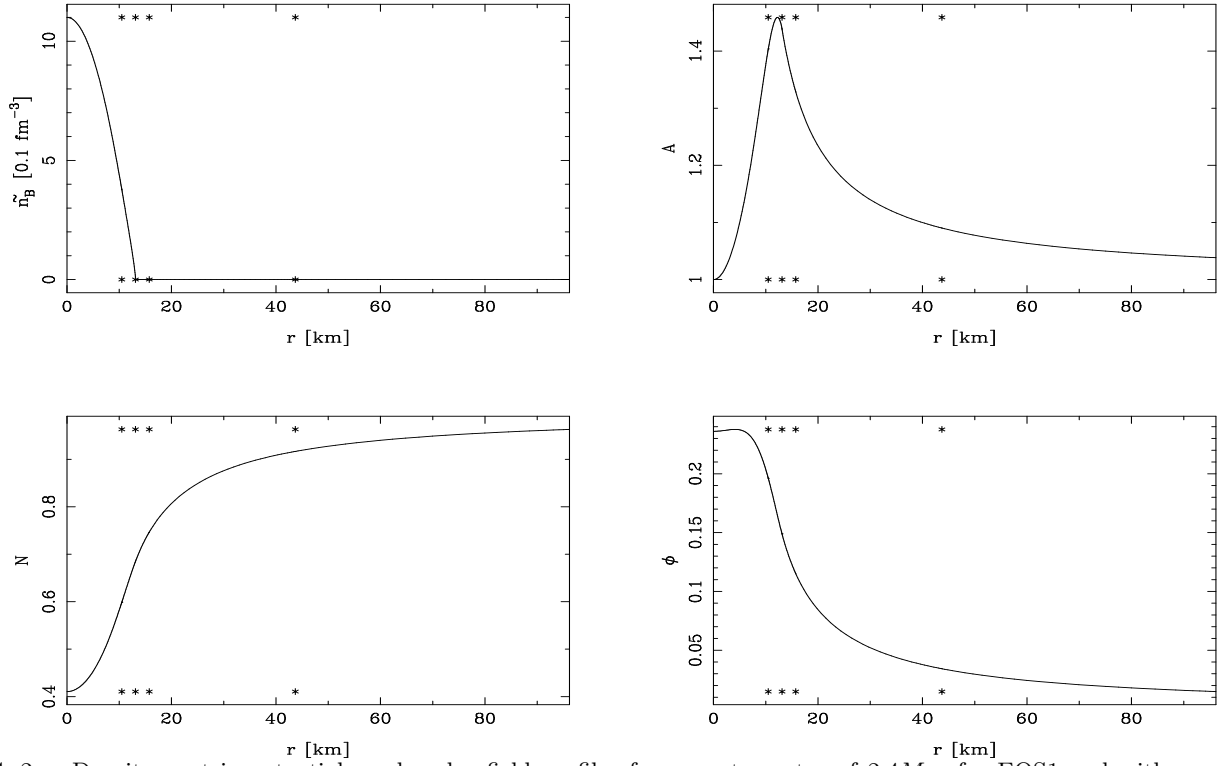


FIG. 2. Density, metric potentials and scalar field profiles for a neutron star of $2.4M_{\odot}$, for EOS1 and with a coupling function $a(\varphi) = \exp(-3\varphi^2)$. The asymptotic scalar field value is $\varphi_0 = 10^{-5}$. Star's radius $R_{star} = 13.1$ km. Stars denote the limits of the different numerical grids.

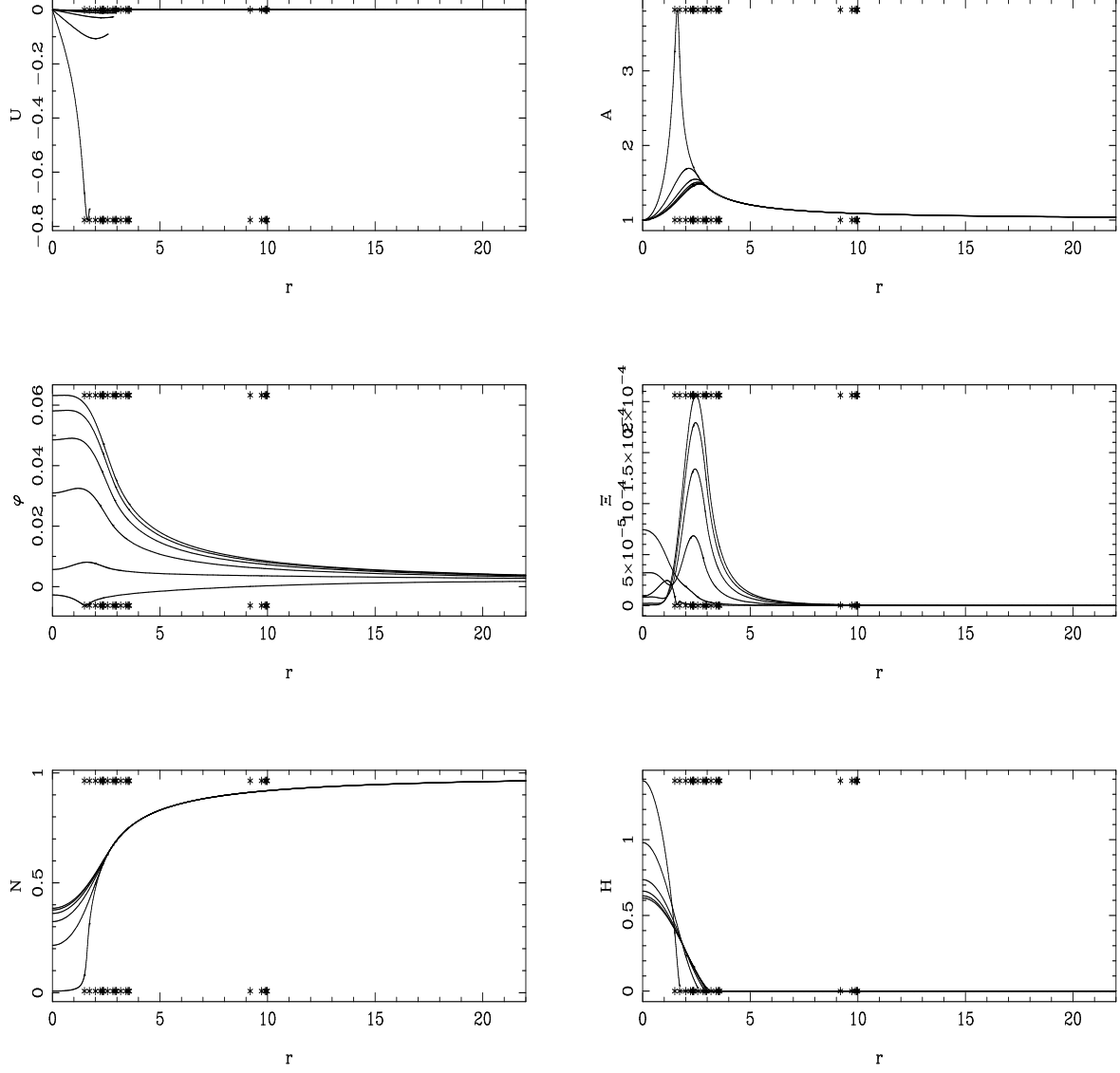


FIG. 3. Profiles of various quantities at different values of t between 0 and 4.64 ms, for collapse A. The radius r is expressed in units of 3.74 km. The fluid velocity is expressed in units of c and its evolution is downward. The extremity of each curve gives the position of the star's surface at the corresponding instant. The evolution for A , Ξ and H is upward, for φ and N is downward. Stars denote the limits of the different numerical grids (moving during collapse).

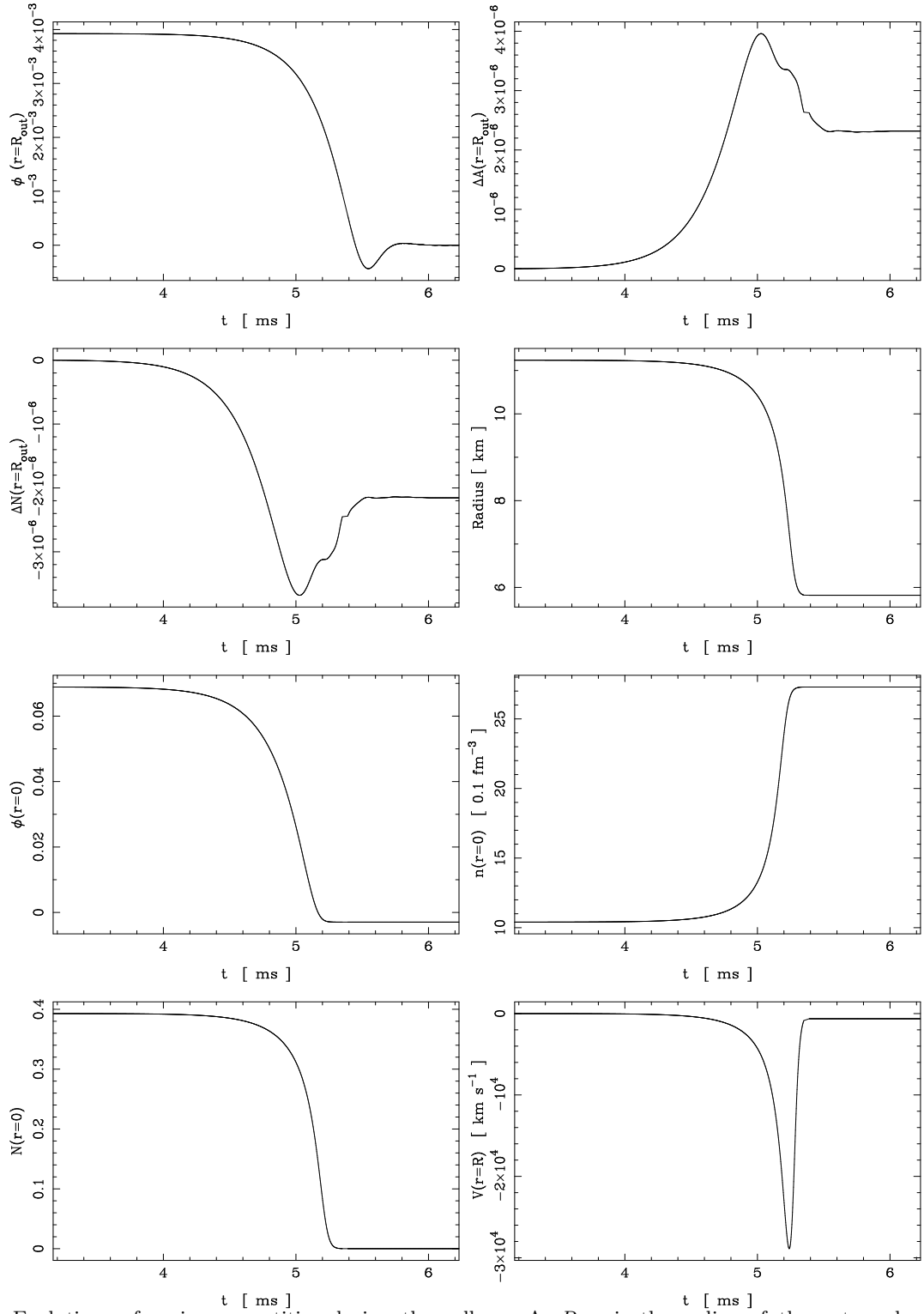


FIG. 4. Evolutions of various quantities during the collapse A. R_{out} is the radius of the outer edge of the grid. $\Delta A = A(t) - A(0)$ and $\Delta N = N(t) - N(0)$ represent the variations of the metric coefficients, $n(r=0)$ is the central baryon density and $V(r=R)$ is the star's surface velocity.

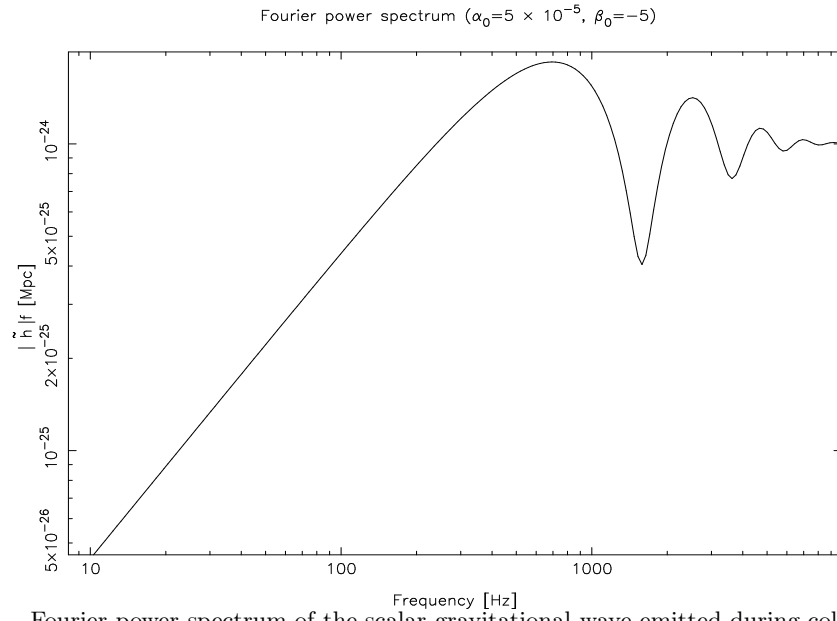


FIG. 5. Fourier power spectrum of the scalar gravitational wave emitted during collapse A.

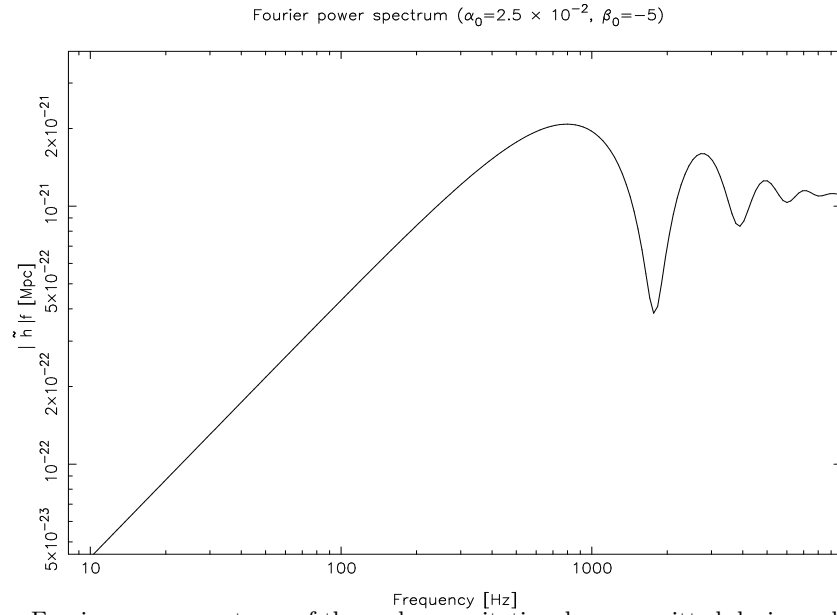


FIG. 6. Fourier power spectrum of the scalar gravitational wave emitted during collapse B.

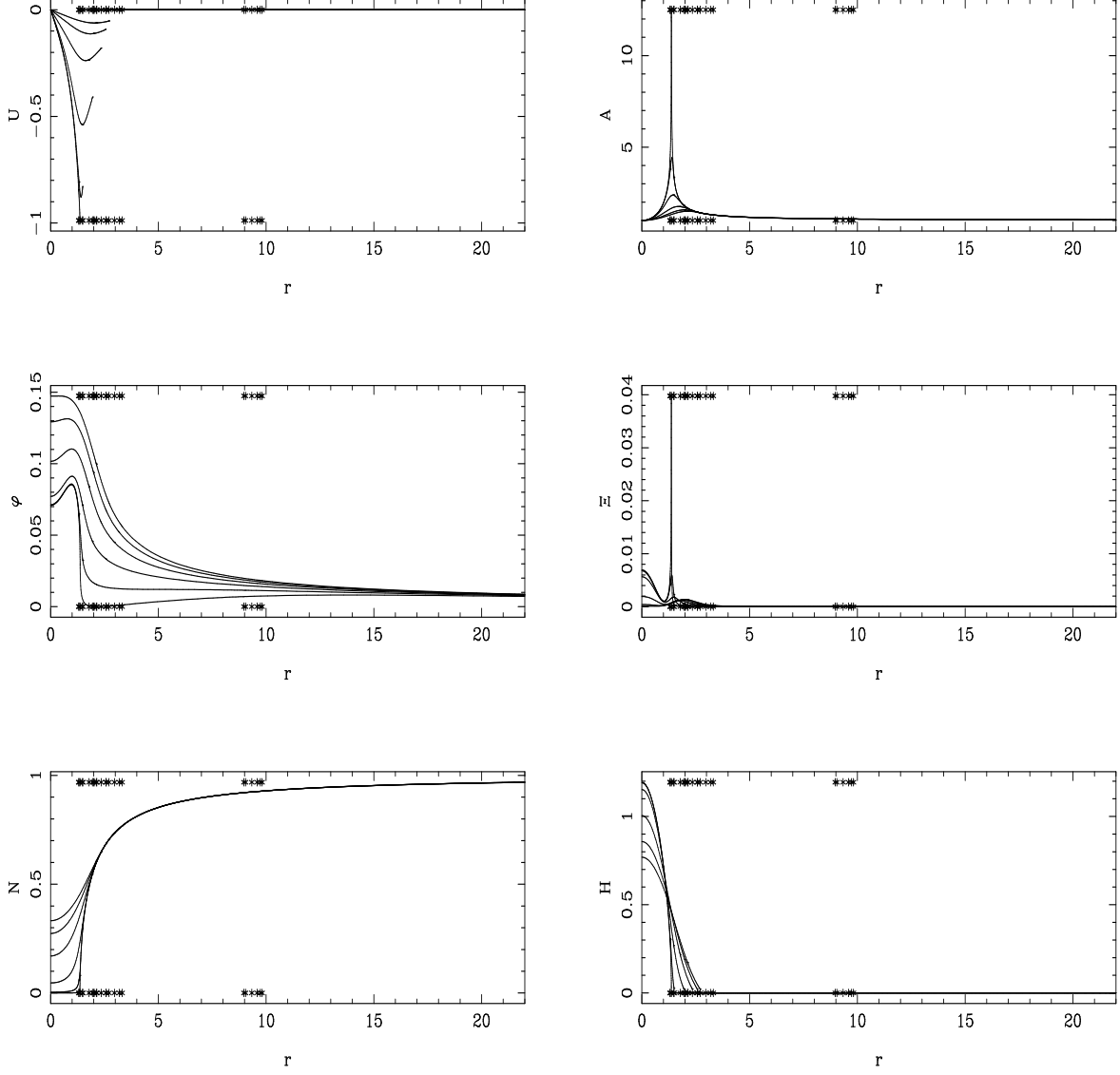


FIG. 7. Profiles of different quantities at different values of t between 0 and 12.22 ms, for collapse C. The radius r is expressed in units of 7.18 km. The fluid velocity is expressed in units of c and its evolution is downward. The extremity of each curve gives the position of the star's surface at the corresponding instant. The evolution for A , Ξ and H is upward, for φ and N is downward. Stars denote the limits of the different numerical grids (moving during collapse).

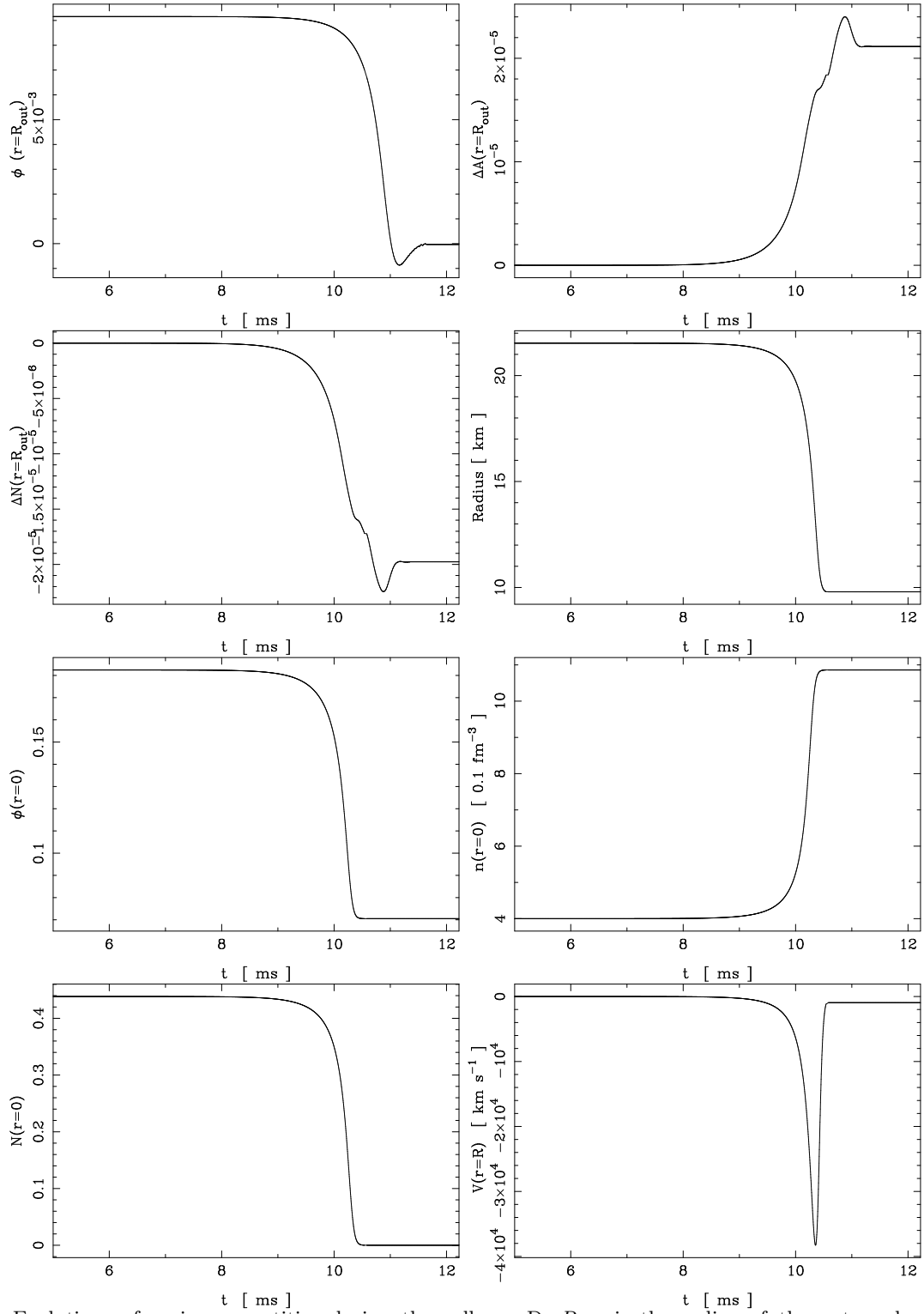


FIG. 8. Evolutions of various quantities during the collapse D. R_{out} is the radius of the outer edge of the grid. $\Delta A = A(t) - A(0)$ and $\Delta N = N(t) - N(0)$ represent the variations of the metric coefficients, $n(r=0)$ is the central baryon density and $V(r=R)$ is the star's surface velocity.

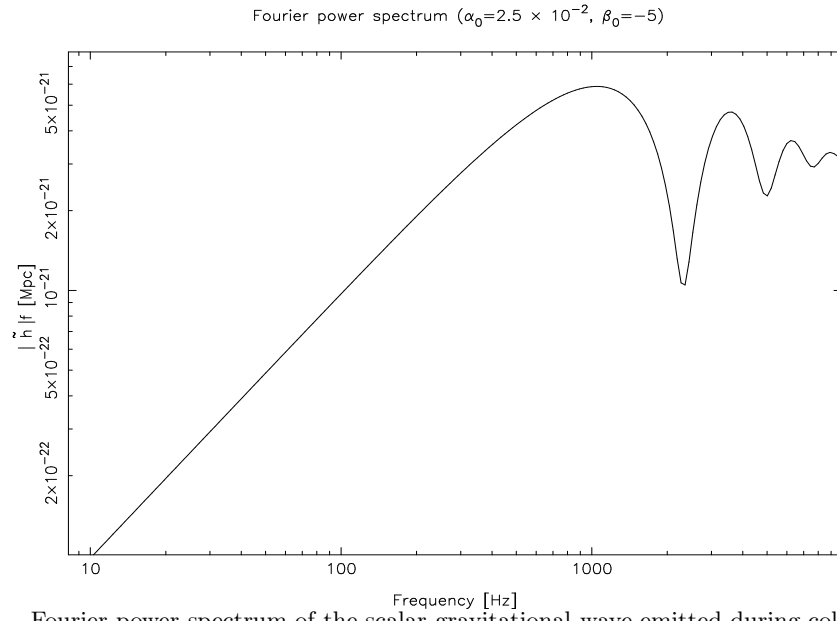


FIG. 9. Fourier power spectrum of the scalar gravitational wave emitted during collapse C.

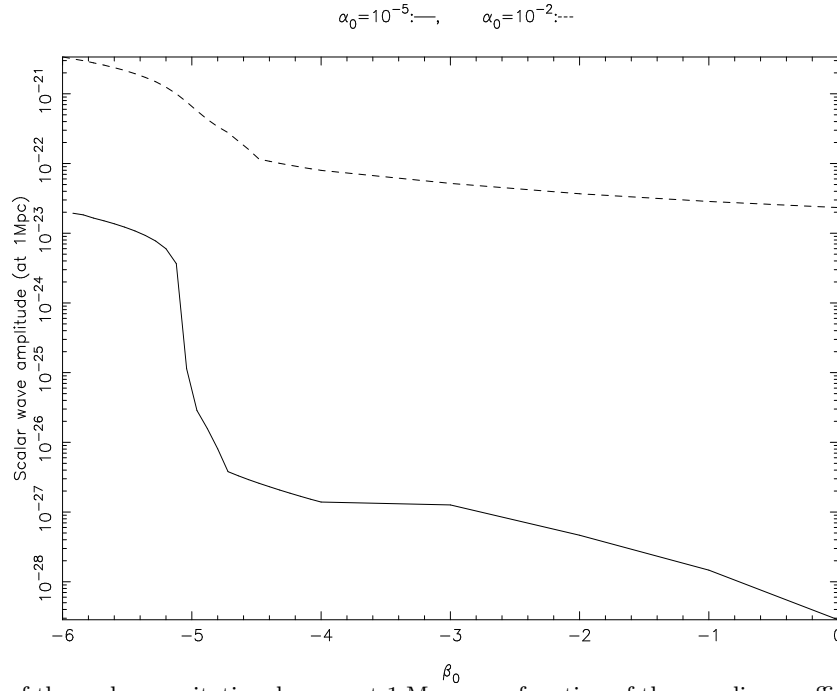


FIG. 10. Amplitude of the scalar gravitational wave, at 1 Mpc, as a function of the coupling coefficient β_0 , for two different values of α_0 .

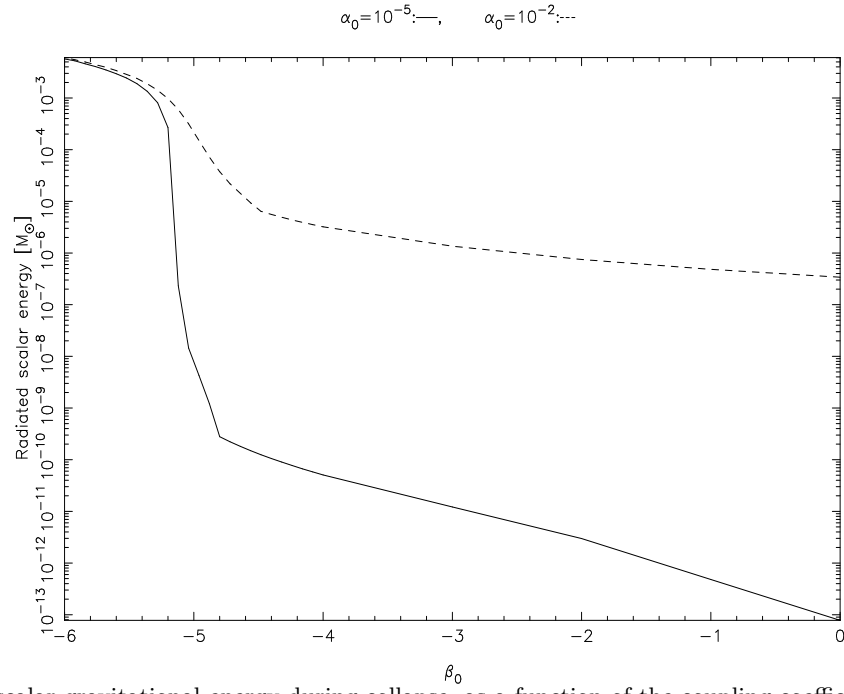


FIG. 11. Radiated scalar gravitational energy during collapse, as a function of the coupling coefficient β_0 , for two different values of α_0 .

TABLE I. Initial condition parameters of the collapses presented in this text. r_{star} denotes star's radius, M_G is the gravitational mass, M_B the baryonic one and ω the scalar charge.

Collapse	EOS	φ_0	α_0	β_0	r_{star} [km]	$\tilde{n}_B(r=0)$ [n_{nuc}]	M_G [M_\odot]	M_B [M_\odot]	ω [M_\odot]
A	1	10^{-5}	5×10^{-5}	-5	11.2	10.4	1.97	2.26	0.204
B	1	10^{-5}	2.5×10^{-2}	-5	11.8	10.4	2.07	2.41	0.484
C	2	10^{-5}	5×10^{-5}	-5	21.5	4	3.31	3.68	0.921
D	2	10^{-5}	2.5×10^{-2}	-5	22.2	4	3.41	3.82	1.16

